J Electroceram (2007) 18:295–303
DOI 10.1007/s10832-007-9165-8

Nanostructured TiO_2-based mixed metal oxides prepared using microemulsions for carbon monoxide detection

Theera Anukunprasert · Chintana Saiwan · Elisabetta Di Bartolomeo · Enrico Traversa

Received: 24 July 2006 / Accepted: 19 April 2007 / Published online: 1 June 2007

Abstract Nanostructured powders of Nb-doped TiO_2 (TN) and SnO_2 mixed with Nb-doped TiO_2 in two different atomic ratios—10 to 1 (TSN 101) and 1 to 1 (TSN 11)—were synthesized using the reverse micelle microemulsion of a nonionic surfactant (brine solution/1-hexanol/Triton X-100/cyclohexane). The powders were characterized by transmission electron microscopy (TEM) and X-ray diffraction (XRD). Thick films were fabricated for gas sensors and characterized by XRD analysis and field emission scanning electron microscopy (FE-SEM). The effects of the film morphology and firing temperature in the range 650–850 °C on CO sensitivity were studied. The best gas response, expressed as the ratio between the resistance in air and the resistance under gas exposure (R_{air}/R_{gas}), was measured for TSN 11 at 11 for 1,000 ppm CO exposure. All types of sensors showed good thermal stability. The electrochemical impedance spectroscopy (EIS) measurements were performed in different gas atmospheres (air, O_2, CO and NO_2) to better understand the electrical properties of the nanostructured mixed metal oxides.

Keywords Nanostructured mixed metal oxides · Microemulsions · Carbon monoxide · Gas sensor

T. Anukunprasert (✉) · C. Saiwan
The Petroleum and Petrochemical College,
Chulalongkorn University,
254 Phyathai Road Patumwan,
10330 Bangkok, Thailand
e-mail: Theeraa@hotmail.com

E. Di Bartolomeo · E. Traversa
Department of Chemical Science and Technology,
University of Rome Tor Vergata,
Via della Ricerca Scientifica 1,
00133 Rome, Italy

1 Introduction

Metal-oxide semiconductor films have been widely studied as sensors for pollutant gases [1–8]. In particular, isostructural single oxides such as TiO_2 and SnO_2 have been investigated and commercialized for toxic gas monitoring [3, 9–12]. However, in some crucial applications, such as combustion exhaust monitoring at high temperatures (above 500 °C), the single oxide sensors show poor performance. For example, at high temperatures, SnO_2 suffers from structure instability and poor selectivity, while TiO_2 sensors show low sensitivity [10]. Therefore, the use of heterometallic oxides (mixed metal oxides or doped metal oxides) has recently emerged as promising for gas sensors because it is possible to combine the best positive sensing properties of each oxide [4, 7, 13–15].

In particular, the mixing of SnO_2 with TiO_2 is a good combination due to their similar crystalline structures (rutile phase) and closed lattice parameters. The phase diagram for the SnO_2–TiO_2 binary composition predicts an immiscibility domain, where favorable conditions are created for spinodal or chemical decomposition (formation between the modulated phase and TiO_2 or SnO_2-rich phases) [16]. The substitution of Sn for Ti in the lattice structure (spinodal region) is proven to aid the formation of solid solutions, alter the structure, and contribute to the thermal stability of TiO_2 [17–22]. This may lead to an improvement in the gas-sensing properties.

On the other hand, it has been observed that doping with suitable cations with low bulk solubility can also modify the electronic properties for gas interaction on the exposed surface as a result of grain boundary and surface segregation [17, 18, 23, 24]. Previous results showed that substitution of cations, such as Nb, Ta, or Cr, can enhance the gas-sensing properties of TiO_2 [25–28]. Nb ions were

Table 1 Conditions for preparation of different atomic ratios of precursors.

Mixed metal oxide types	1.5 M of $TiCl_4$, (ml)	$SnCl_4$ (g)	$NbCl_5$ (g)
3% Nb-doped TiO_2 (TN)	5.0	–	0.06079
3% Nb-doped TiO_2 mixed with SnO_2 by ratio 1 to 1 (TSN 11)	5.0	2.62935	0.06079
3% Nb-doped TiO_2 mixed with SnO_2 by ratio 10 to 1 (TSN 101)	5.0	0.26294	0.06079

All components were mixed in diluted HCl solution for preparation of 25 ml aqueous phase.

found to affect the equilibrium reaction between the point defects in the bulk of sensing materials, thus enhancing the gas-sensor performance [25–32]. Besides the effect of surface defects, Ta^{+5} or Nb^{+5} dopants can also reduce the number of oxygen vacancies, thus retarding the phase transition of TiO_2 from anatase to rutile [11, 25, 26, 29, 30].

The physical properties of a gas sensor can be improved by reducing the size of the metal oxides to nano-meter scale [33]. One reason is that the surface-to-bulk ratio for the nano-sized metal oxides is much larger than that of bulk metal oxides, leading to an enhancement of surface properties. Another reason is that the conduction type of the metal oxide is determined by grain size. When the grain size (D) is small enough ($D<2L$, where L is the space-charge depth), the metal oxide resistivity is determined by grain control, and the conduction becomes a surface conduction [34–42].

The aim of this work, therefore, is an attempt to merge both the advantages of mixed metal oxides and nano-crystalline materials for better sensing properties of gas sensors. Our previous studies showed interesting results using microemulsions of an anionic surfactant for synthesizing nanostructured Nb-doped TiO_2 [43, 44]. However, NaCl needs to be added to the system to control the microstructure of reverse micelles. This leads to difficulty in synthesizing complex systems of heterometallic oxides (more than three metal oxides), and sometimes causes impurity in the synthesized powders. Thus, microemulsions using a nonionic surfactant instead of the ionic surfactant [44] were studied as an alternative, and as an effective method of synthesizing such complex types of metal oxides. The nanostructured metal oxides were characterized, and the sensing properties are presented here.

2 Experimental

2.1 Metal oxide preparation

A high purity nonionic surfactant (TX-100) and 1-hexanol (+98%) were obtained from Fluka (Switzerland). The analytical reagents (AR), consisting of 99.0% cyclohexane as an oil phase and 99.5% acetone, were purchased from Lab-Scan (Thailand). Ammonium hydroxide (NH_4OH, AR grade) was purchased from J.T.Baker (USA), and niobium (V) chloride and tin (IV) chloride pentahydrate from Sigma-Aldrich (Germany). Titanium dioxide (TiO_2, P25) was obtained from Degussa (Germany) and 40% hydrofluoric acid (HF) from Riedel-Haën (Germany). Perchloric acid (56%, $HClO_4$) was purchased from Carlo Erba (Italy). Hydrochloric acid (36.46 wt.% wt, HCl) was obtained from VRW (England). All reagents were used without further purification. Deionized water was used throughout the experiments.

The mixed metal oxides were prepared with the following compositions (Table 1): 3% Nb-doped TiO_2 (TN), 3% Nb-doped TiO_2 mixed with SnO_2 in a ratio of 1 to 1 (TSN 11), and 3% Nb-doped TiO_2 mixed with SnO_2 in a ratio of 10 to 1 (TSN 101).

A titanium tetrachloride solution ($TiCl_4$) in concentrated HCl was prepared by dissolving and heating TiO_2 in a concentrated aqueous HF solution until a clear solution was obtained. Then a few milliliters of $HClO_4$ were added to remove excess HF from the solution. Finally, titanium tetrachloride in concentrated HCl solution was obtained by adding HCl.

The oil phase was prepared by mixing 66.78 g of the nonionic surfactant, TX-100, and 53.00 g of *n*-hexanol with 210.33 g of cyclohexane. The solution was then mildly stirred for 30 min. For the aqueous phase, the preparation

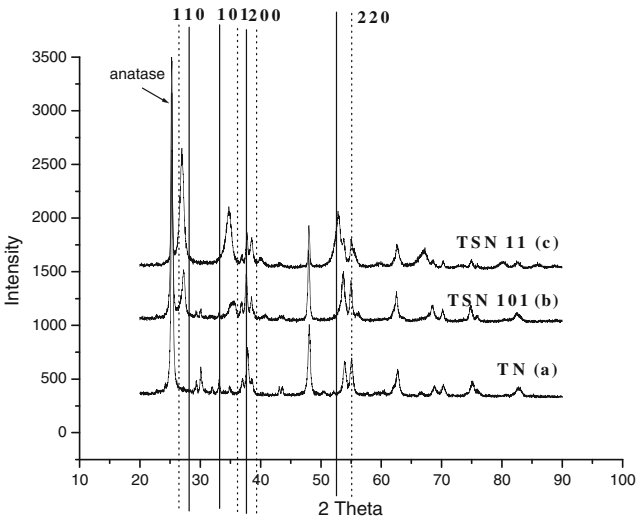

Fig. 1 XRD pattern of TN (**a**), TSN 101 (**b**) and TSN 11 (**c**) powders calcined at 650 °C. The *dotted* and the *solid lines* represent the specific plane of SiO_2 and TiO_2, respectively

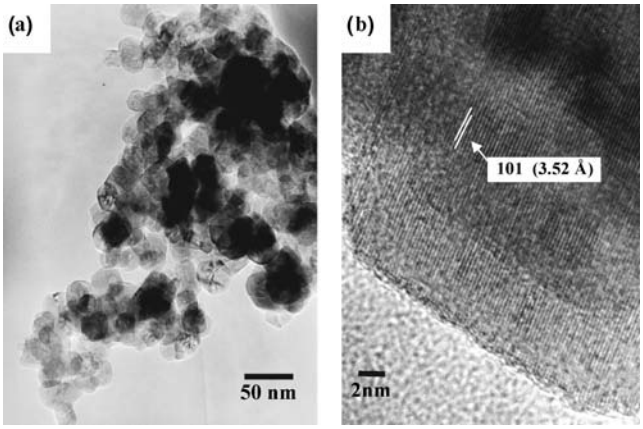

Fig. 2 TEM image of Nb-TiO_2 powder (**a**) and HR-TEM (**b**) of anatase structure (plane 101) of TiO_2 calcined at 650 °C

was performed under N_2 atmosphere. This phase was prepared by weighing appropriate amounts of $NbCl_5$ and $SnCl_4$ pentahydrate, followed by the addition of 10 ml of 36.46 wt.% of HCl and 5 ml of 1.6 M $TiCl_4$, and then adding deionized water until 25 ml of solution was obtained (Table 1). After the addition of 3.84 ml of aqueous phase in the string oil phase, a microemulsion was formed in a few seconds, which was indicated by a clear solution. The microemulsion was continuously stirred and equilibrated at 30 °C for 1 day. After that, the precipitation of the microemulsion was carried out by bubbling ammonia, prepared by bubbling air through a concentrated NH_4OH solution, into the microemulsion. During the precipitation, the temperature was controlled at 30 °C. The as-synthesized mixed oxide was separated by a high-speed centrifuge at 10,000 rpm. It was then washed with cyclohexane, twice with ethanol and acetone, and finally by water to remove the remaining surfactant from the as-synthesized particles. The as-synthesized mixed oxide was dried and calcined for 5 h at 650 °C.

2.2 Sensor fabrication

Thick-film sensors were fabricated by suspending the oxide powders, TN, TSN 101 and TSN 11, with printing oil and depositing the resulting slurry on an alumina substrate with screen-printed comb-type Au electrodes (3 mm width, 0.2 mm spacing). The samples were fired at 650, 750 and 850 °C.

2.3 Materials characterization

The phase analysis of the powders was performed by using an X-ray diffractometer (XRD, Phillips X-Pert Pro 500) at room temperature. Peak positions were compared with the standards to identify the crystalline phases. The size and shape of the particles were observed using a transmission electron microscope (TEM, Jeol 2010, Tokyo, Japan). The effect of firing temperature on the phase transformation of the metal oxide films on alumina substrates was studied by XRD in thin film mode, and the morphology of the films was observed by field emission scanning electron microscopy (FE-SEM, Leo Supra 35).

2.4 Gas sensing measurements

The gas sensing characteristics were examined in a conventional gas-flow apparatus equipped with a controlled heating facility. The voltage was applied at 15 V for DC measuring, using a programmable voltage source (230 Keithley). The sensors were alternatively exposed to air or CO (20–1,000 ppm in air) at the total flow rate of 200 ml/min, at 550 °C. The films were left under 550 °C with 5 ml/min air flow rate overnight before sensing CO. The current was measured using a system electrometer (Keithley 6514). After CO was applied into the flow system, an increase in the conductivity of the metal oxides was observed, and thus an increase in current was detected. The step response was observed by switching the flow from air to gas and gas to air. The gas response is defined as the ratio of R_{air}/R_{gas} where R_{air} and R_{gas} are the resistances in air and under gas exposure, respectively, in the case of n-type semiconductors. A thermocouple very close to the surface of the sensor was used during the measurements to monitor any thermal heating due to the applied voltage. No temperature increase was ever recorded.

Impedance measurements were performed in a frequency domain between 0.01 and 10^7 Hz using a frequency response analyzer (Solartron 1260). The impedance study of the TSN 11 and TSN 101 films was carried out at 550 °C, the same temperature that was used for DC gas measurements. The sensors were exposed to both oxidizing and reducing gases (air, O_2, 1,000 ppm of CO in air and 1,000 ppm of NO_2 in air).

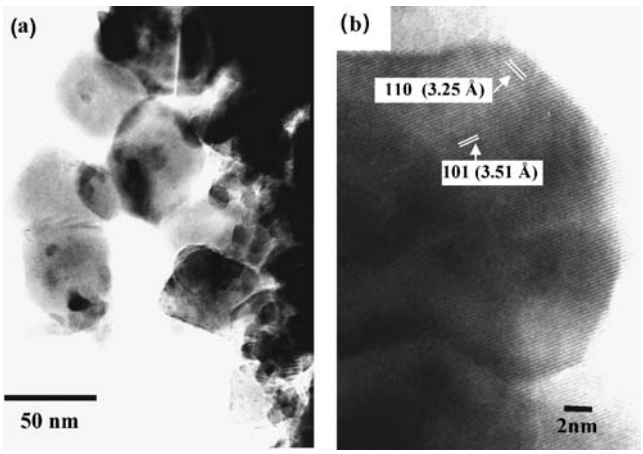

Fig. 3 TEM image of TSN101 powder (**a**) and HR-TEM (**b**) of solid solution of SnO_2 mixed TiO_2 calcined at 650 °C

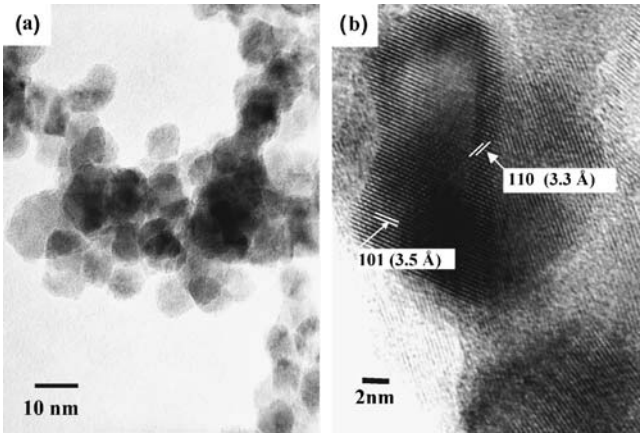

Fig. 4 TEM image of TSN11 powder (**a**) and HR-TEM (**b**) of solid solution of SnO_2 mixed TiO_2 calcined at 650 °C

3 Results and discussion

3.1 Structural and microstructural analysis of powders

Results obtained for pure TiO_2 and Nb–TiO_2 prepared using microemulsions with ionic surfactants have been reported in previous papers [43, 44]. Briefly, pure TiO_2 clearly showed a phase transformation from anatase to rutile structure at 650 °C, while Nb–TiO_2 was present in anatase phase even at 850 °C. In this present work, the previous findings were compared with the XRD patterns of TN, TSN 11, and TSN 101 powders prepared at 650 °C (Fig. 1). The XRD pattern of TN showed only the anatase (d=3.53 Å, 2θ=25.7 °) structure at 650 °C. This result confirmed the effect of Nb in stabilizing the anatase structure, in agreement with the relevant literature [29–32, 44]. For TSN 11 and TSN 101, no rutile (d=3.2 Å, 2θ=27.5 °) phase was observed as well, even though the anatase structure was observed together with a solid solution between SnO_2 and TiO_2 rutile structures at 2θ between 26.5 and 27.5 ° (plane 110). The crystal size of the powders was determined from TEM images. Figure 2 shows that the TN powder featured uniform grains in anatase structure with the characteristic plane 101 at a distance d=3.52 Å. The measured average crystal size was 14 nm. For TSN 101, two different mean crystal sizes, 50 and 10 nm, were present (Fig. 3). High resolution TEM (HR-TEM) revealed a slight shift in the d-spacing of the anatase structure (plane 101 at d=3.51 Å); moreover the d-spacing of the characteristic plane 110 for the solid solution between SnO_2 and TiO_2 was measured at d=3.25 Å. For TSN 11, the TEM results (Fig. 4) showed very fine and uniform grains with a mean crystal size of 10 nm. HR-TEM allowed for the measurement of the d-spacing at 3.3 Å, typical of the SnO_2–TiO_2 solid solution. Thus, the larger the atomic ratio of Sn to Ti, the larger the observed d-spacing. This shift indicated the formation of a solid solution between TiO_2 and SnO_2 [20, 21, 39]. The formation of both anatase phase and solid solution can be explained, as indicated in the literature [20, 21, 39], in that chemical decomposition (formation between the modulated phase and TiO_2 or SnO_2-rich phases) can occur if the condition does not favor thermodynamic or equilibrium conditions, which can easily occur in the fast precipitation (less than 60 s) of the microemulsion environment.

The finest crystal size was obtained for TSN 11, while the largest for the TSN 101, where two different crystal sizes were present. The difference in mean crystal size of the mixed oxides may correspond to the kinetics of

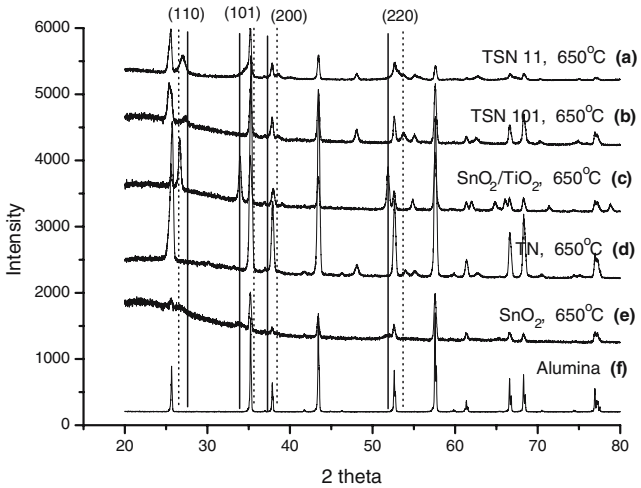

Fig. 5 XRD pattern of the following films fired at 650 °C: TSN 11 (**a**), TSN 101 (**b**), SnO_2 mixed Nb-TiO_2 with 1:1 ratio (**c**), Nb-TiO_2 (**d**), SnO_2 (**e**) and alumina substrate (**f**). The *dotted* and the *solid lines* represent the specific plane of SiO_2 and TiO_2, respectively

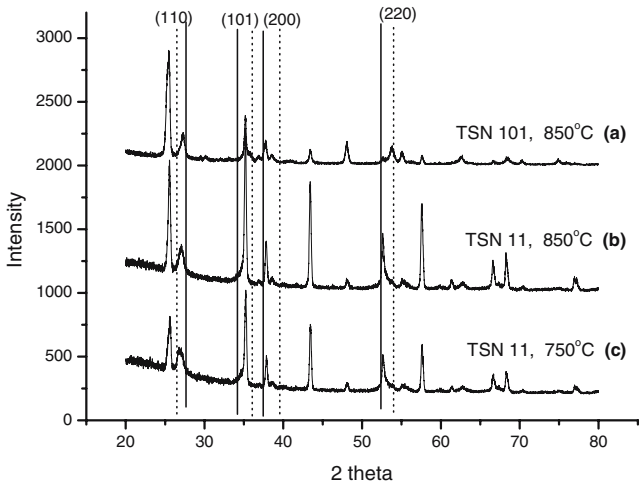

Fig. 6 XRD pattern of: TSN 101 film fired at 850 °C (**a**), TSN 11 films fired at 750 ° (**b**) and 850 °C (**c**), respectively. The *dotted* and the *solid lines* represent the specific plane of SiO_2 and TiO_2, respectively

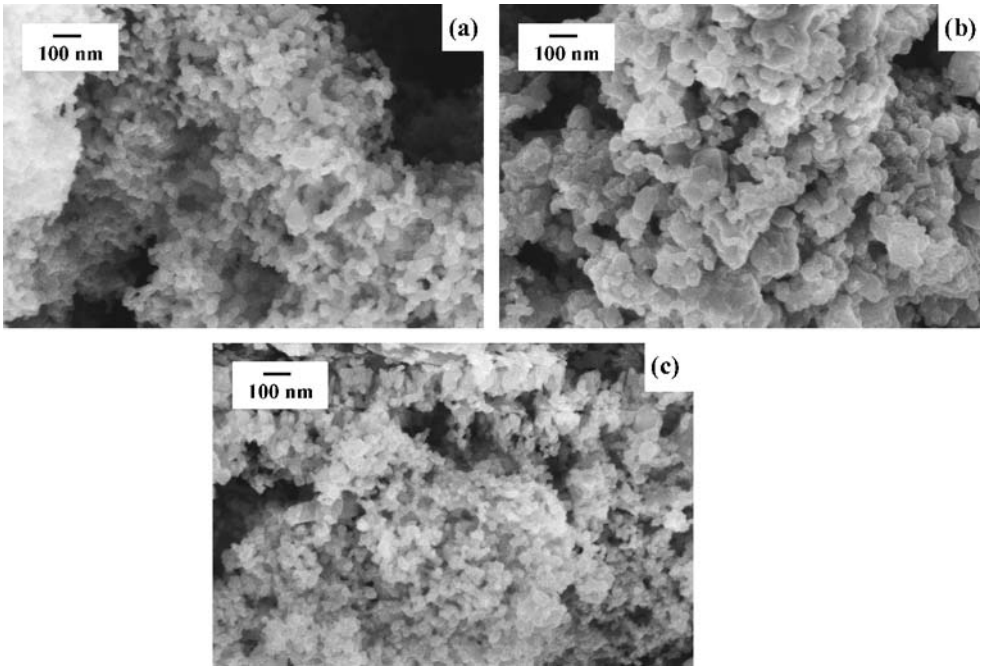

Fig. 7 SEM images of: TN (**a**), TSN 101 (**b**) and TSN 11 (**c**) films all fired at 650 °C before CO gas measurements

precipitation in the micro-environment of reverse micelles. Although the precipitation kinetics is very fast and hard to observe, literature has suggested that increasing the metal concentration enhances the nucleation, thus decreasing the size of the metal oxide particles [45]. In our experiments, the concentrations of $TiCl_4$ and $NbCl_5$ were kept constant while the $SnCl_4$ concentration was varied at 0.15 and 1.5 M for TSN 101 and TSN 11, respectively. Thus, the total metal concentration increased with increasing the ratio of the Ti/Sn. Therefore, a smaller crystal size was observed for TSN 11.

3.2 Structural and microstructural analysis on thick-film sensors

Figure 5 shows the XRD patterns of TN, TSN 101, and TSN 11 films after firing at 650 °C. For sake of comparison, single oxide (SnO_2) and a physically mixed SnO_2/Nb-doped TiO_2 sample obtained from the microemulsion in the 1 to 1 atomic ratio (SnO_2/TiO_2) were also prepared. The reference pattern of the bare alumina substrate is also reported in Fig. 5(f).

The crystal sizes of all the films were also determined using the Scherrer formula, but no significant changes in crystal size were observed after firing, with respect to the starting powders. The TN sample fired at 650 °C showed the presence of only TiO_2 in anatase structure (Fig. 5(d)), as expected [31, 43, 46, 47]. The anatase stabilization is due to the effect of Nb^{+5} substituting Ti^{+4} in the crystalline lattice, which reduces the number of oxygen vacancies, thus

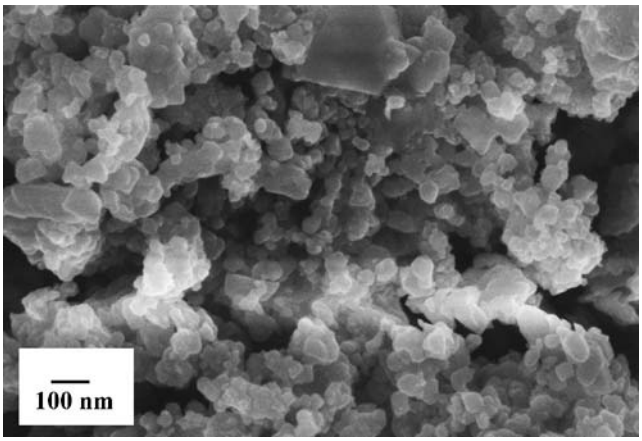

Fig. 8 SEM image of TSN 101 film after CO gas measurements

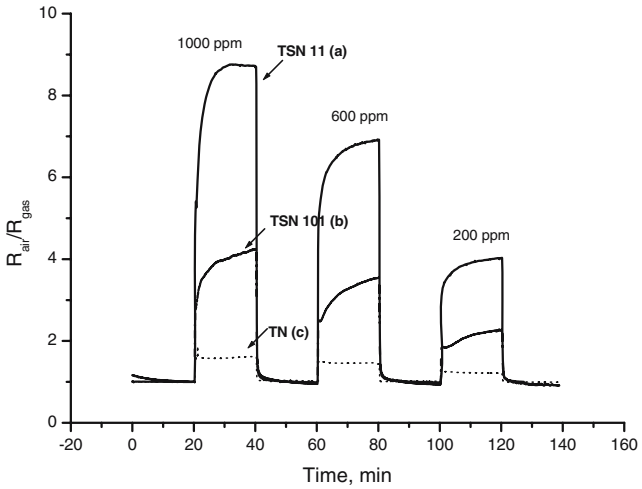

Fig. 9 Sensor response of TSN 11 (**a**), TSN 101 (**b**) and TN (**c**) fired at 650 °C to different CO concentrations (200–1,000 ppm in air) at 550 °C with an applied voltage of 15 V

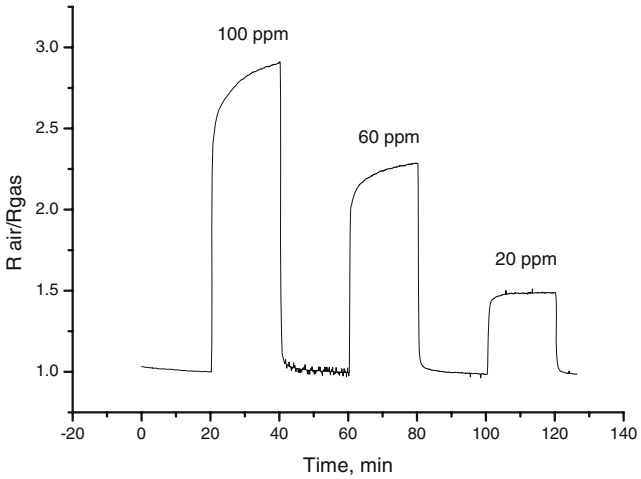

Fig. 10 Sensor response of TSN 11 fired at 650 °C to 20–100 ppm CO at 550 °C with an applied voltage of 15 V

retarding the anatase-to-rutile transformation and grain growth.

Nb stabilized the anatase structure in all the samples TN, TSN 101, and TSN 11. The XRD patterns of TSN 101 and TSN 11 indicated the presence of both the anatase phase (d=3.52 Å, 2θ=25.3 °) and the TiO_2–SnO_2 solid solution (d=3.25–3.3, 2θ=26.5 °–27.5 °, plane 110). The XRD patterns of the films prepared with SnO_2 (Fig. 5(e)) and with mixed SnO_2/TiO_2 powders (external mixing, Fig. 5(c)) showed only the peaks of each single oxide, SnO_2 and TiO_2. No solid solution for the mixed SnO_2/TiO_2 sample was observed. Firing at temperatures above 650 °C did not modify the anatase phase and solid solution peaks for the films obtained from microemulsion-derived powders, even up to 850 °C [43] (Fig. 6(a)–(c)).

Figure 7 is the SEM micrographs of TN (a), TSN 101 (b), and TSN 11 (c) thick films, all fired at 650 °C, before the gas exposure. All sensors showed a porous morphology. TN and TSN 11 films had very fine and uniform particles, whereas the TSN 101 clearly showed grains with two different sizes. This may correspond to the two different phases (anatase and solid solution) that were also observed from the TEM results. The morphology of all thick films was also investigated after the CO exposure. SEM images showed no changes in grain size for TN and TSN 11 films, even after a long exposure (a few weeks) to CO gas at 550 °C. However, a weak grain size increase was observed for the TSN 101 thick film, as reported in Fig. 8.

3.3 CO sensing response

Figure 9 shows the CO response at 550 °C of TN (a), TSN 101 (b), and TSN 11 (c) films fired at 650 °C to different gas concentrations. For the TN sensor, the largest gas response was 1.6 for exposure to 1,000 ppm of CO. In comparison to our previous work on Nb–TiO_2 synthesized using an anionic surfactant [43], the sensitivity of the TN sensor was slightly smaller. In the case of sensors based on powders obtained with anionic surfactants, the gas response was 2.2 at the same temperature and gas concentration [43]. This fact can be explained by the smaller grain size, 6 nm, and thus the larger surface areas of these powders compared to the mean grain size, 14 nm, of the TN powders.

The TSN 101 sensor showed good gas response at all gas concentrations. The largest response was 4.3 for 1,000 ppm of CO. This value is more than 3 times larger than the gas response obtained for the TN films. Even though the grain size of the TSN 101 was larger than the TN, the gas response of the TSN 101 sensor was higher. This might be due to the effect of the additional phase (the mixed solid solution structure) that enhanced the gas response of the pure anatase structure. For the TSN 11 sensor, a fast and large gas response to different CO concentrations was obtained. The largest gas response was almost 9 for 1,000 ppm of CO. This value is almost seven times larger than that of the TN film. Because of this good gas response, the lower gas concentration range (20–100 ppm of CO in air) was investigated and the results are reported in Fig. 10. It was found that the TSN 11 film still showed a gas response of 1.5 for a concentration of 20 ppm of CO. The best sensitivity of the TSN 11 film is in agreement with the structural and microstructural investigations.

To study the effects of firing temperature on the gas response of the films, the TSN 11 sensors were heated to 750 and 850 °C. Figure 12 shows the sensor response at

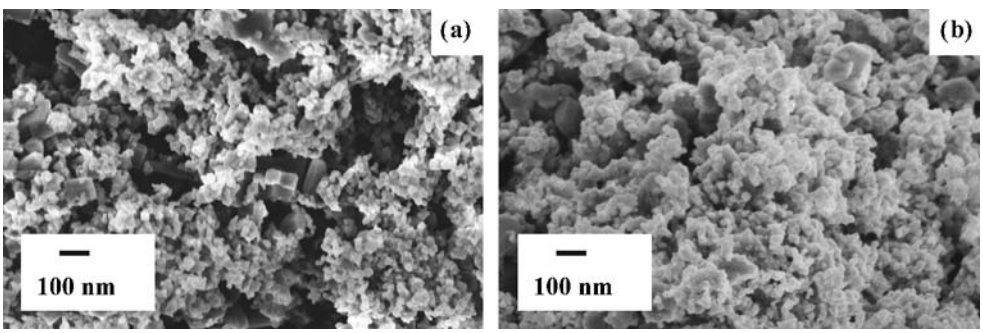

Fig. 11 SEM micrographs of TSN 11 sensors fired at 850 °C (**a**) before CO gas measurements and (**b**) after CO gas measurements at 550 °C

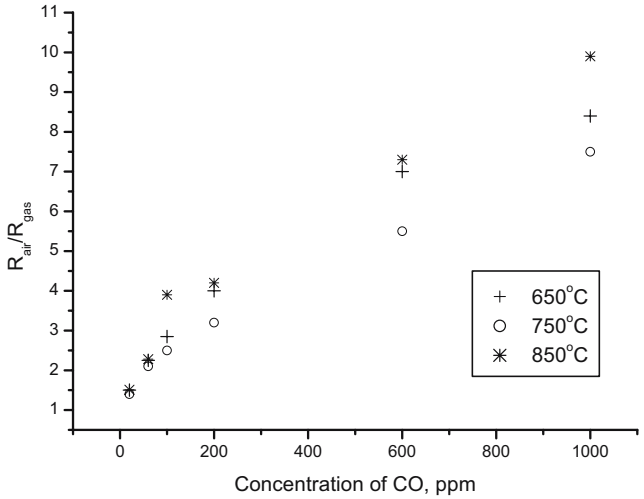

Fig. 12 Sensor response of TSN 11 sensors fired at 650, 750 and 850 °C to different CO concentrations

550 °C of the TSN 11 films fired at 650, 750, and 850 °C, in the CO concentration range between 20 and 1,000 ppm. The result showed that all TSN 11 films presented high thermal stability, even if fired at high temperature. The largest gas response, almost 10, was found for the film fired at 850 °C in the presence of 1,000 ppm of CO. The SEM images, shown in Fig. 11, confirm that the morphology of the film fired at 850 °C did not change and the grain size was still in the nano-meter scale, even after the gas measurements at 500 °C.

In order to highlight the improvement of the sensor performance using a combination of single metal oxides (such as Nb–TiO_2 and SnO_2), SnO_2 was synthesized using the same conditions and system of the non-ionic surfactant. SnO_2 sensors were prepared and fired at 650 °C (Fig. 12). Moreover, the gas response of the TSN 11 obtained from microemulsion was also compared to the response of the

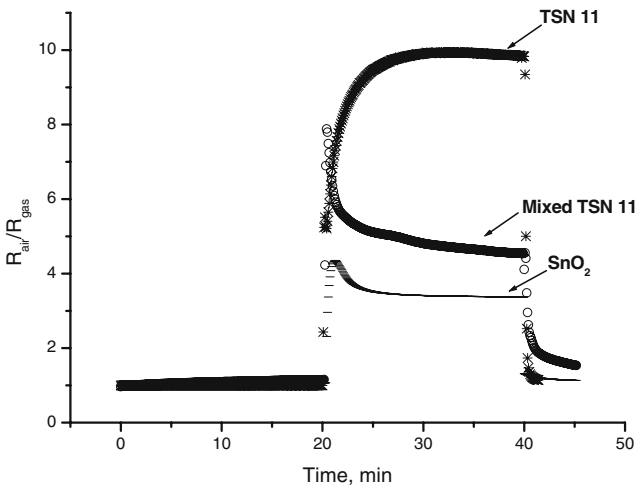

Fig. 13 Response to 1,000 ppm of CO at 550 °C of SnO_2 fired at 400 °C, mixed TSN 11 fired at 850 °C, and TSN 11 prepared from microemulsion (TSN 11, ME) fired at 850 °C

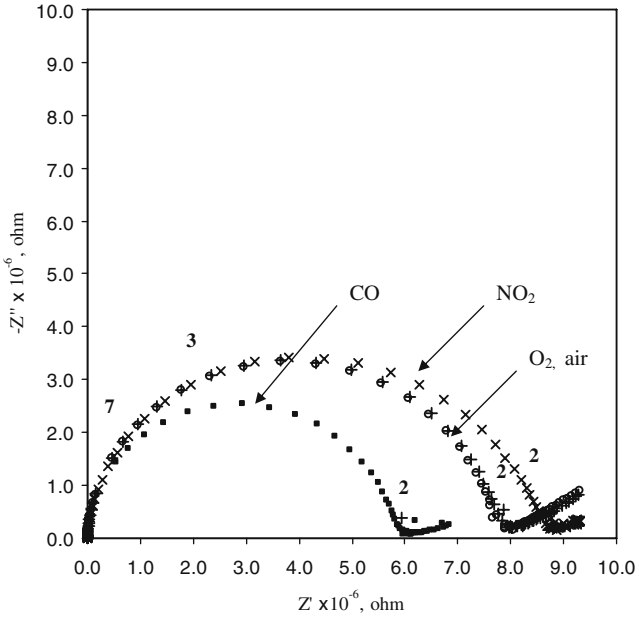

Fig. 14 Nyquist plot of TSN 11 film fired at 550 °C. The numbers above the spectra correspond to the logarithm of the measurement frequencies

TSN 11 obtained by simply mixing the two single oxides in a 1:1 weight ratio (TSN 11 M). Both TNS 11 and TSN 11 M sensors were fired at 850 °C. Figure 13 shows the gas response to 1,000 ppm of CO at 550 °C of SnO_2, TSN 11 obtained from microemulsion, and TSN 11 obtained from mixing, respectively. The gas response of TSN 11 based sensors obtained from microemulsion was the largest and the more stable. The gas response was almost two times the

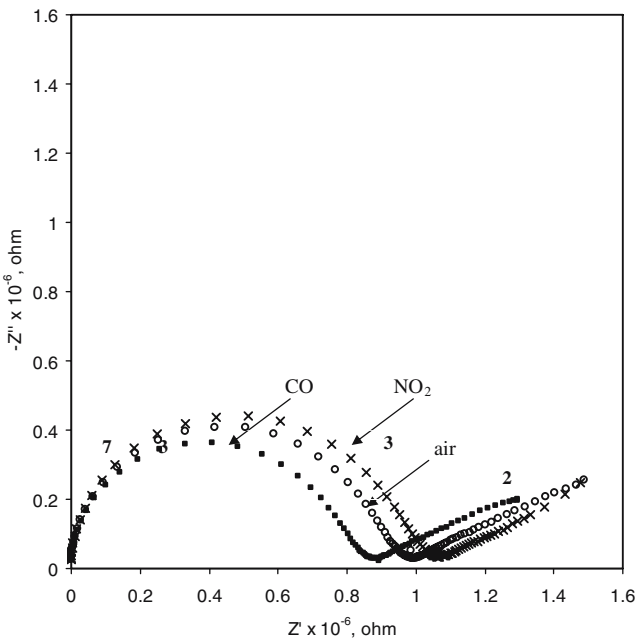

Fig. 15 Nyquist plot of TSN 101 film fired at 550 °C. The numbers above the spectra correspond to the logarithm of the measurement frequencies

response of the TSN 11 obtained by mixing the two oxides. This is further evidence that the solid solution phase observed in the TNS 11 obtained by microemulsion may enhance response and thermal stability.

To better understand the nanostructured mixed metal oxide electrical properties, electrochemical impedance spectroscopy (EIS) measurements were performed. Figures 14 and 15 show the impedance measurements, in Nyquist representation, on the TSN 11 and TSN 101 sensors at 550 °C in the presence of different atmospheres (air, O_2, 1,000 ppm of CO, and NO_2 in air). In both cases, at high frequency, a depressed arc followed by a not-well-defined arc and linear behavior at low frequency were observed. Both for the TSN 11 and the TSN 101 sensors, the high frequency semicircle increased (decreased) in the presence of an oxidizing (reducing) gas. Thus, the total resistance of the sensors increased in the presence of NO_2 and decreased in the presence of CO, in accordance with the behavior of an n-type semiconductor and to the DC-voltage gas response previously reported. No significant difference was observed in the impedance spectra in air and in pure O_2. The high frequency semicircle can be interpreted with the classic series circuit of two parallel resistance-constant phase elements (CPE). According to literature [48–53], only one semicircle is found for the nanometric ceramics, because bulk and blocking grain boundary responses overlap. The low frequency contributions are due to electrode reactions; in particular, the linear behavior can be attributed to the electrode polarization. This is in accordance with the low ionic conductivity at high oxygen concentration and low temperature of anatase phase of titania claimed by some authors [48–50]. It must be also taken into account that the sensors are made of very porous powders deposited on gold electrodes. Moreover, the linear behavior at low frequency is more evident for the TSN 101 sensor, which contains a larger amount of doped titania in comparison to tin dioxide, which is definitively a pure electronic conductor.

4 Conclusions

Reverse micelles microemulsion of a nonionic surfactant (brine solution/1-hexanol/Triton X-100/cyclohexane) was an effective way to produce nanostructured mixed metal oxides. The addition of Nb into TiO_2 was found to stabilize the anatase phase and mean crystal size. On the other hand, the addition of Sn into the nanostructure of TiO_2 caused the formation of solid solution between TiO_2 and SnO_2 with good thermal stability. The morphology and phases of nanostructured mixed oxides have a significant effect on CO gas sensing. It was found that the gas sensitivity improved with the presence of the mixed solid oxide solution and with decreasing the grain size. Therefore, in order to improve the gas-sensing properties of the metal oxides, not only the grain size but also the phase and thermal stability of powder can play an important role. This improvement can be achieved by the right combination of mixed metal oxide powders.

Acknowledgments This work was financially supported by the Golden Royal Jubilee Program, the Thailand Research Fund. The authors would like to express sincere thanks to the National Metal and Materials Technology Centre, Thailand, for the characterization using TEM.

References

1. M.C. Carotta, G. Martinelli, L. Crema, M. Gallana, M. Merli, G. Ghiotti, E. Traversa, Sens. Actuators B **68**, 1 (2000)
2. S.S. Sunu, E. Prabhu, V. Jayaraman, K.I. Gnanasekar, T.K. Seshagiri, T. Gnanasekaran, Sens. Actuators B **101**, 161 (2004)
3. P.K. Dutta, M. Frank, G.W. Hunter, M. George, Sens. Actuators B **106**, 810 (2005)
4. A. Ruiz, J. Arbiol, A. Cirera, A. Cornet, J.R. Morante, Mater. Sci. Eng. C **19**, 105 (2002)
5. S.V. Patel, J.L. Gland, J.W. Schwank, K.D. Wise, M. Zanini-Fisher, Sens. Actuators B **42**, 205 (1997)
6. K.R. Sharma, M.C. Bhatnagar, Sens. Actuators B **56**, 215 (1999)
7. J. Sheng, N. Yoshida, J. Karasawa, T. Fukami, Sens. Actuators B **41**, 131 (1997)
8. J. Zhang, K.H. Au, Z.Q. Zhu, S. O'Shea, Opt. Mater. **26**, 47 (2004)
9. M. Batzill, U. Diebold, Prog. Surf. Sci. **79**, 47 (2005)
10. P.I. Gouma, P.K. Dutta, M.J. Mills, Nanostruct. Mater. **11**, 1231 (1999)
11. M.C. Carotta, M. Ferroni, S. Gherardi, V. Guidi, C. Malagù, J. Eur. Ceram. Soc. **24**, 1409 (2004)
12. L. Sun, L. Huo, H. Zhao, S. Gao, J. Zhao, Sens. Actuators B. **114**, 387 (2006)
13. R.K. Sharma, M.C. Bhatnagar, G.L. Sharma, Sens. Actuators B. **45**, 209 (1999)
14. H. Zou, Y.S. Lin, Appl. Catal. A **265**, 35 (2004)
15. A.M. Ruiz, A. Cornet, K. Shimanoe, J.R. Morante, N. Yamazoe, Sens. Actuators B **109**, 7 (2005)
16. K. Zakrzewska, Thin Solid Films **391**, 229 (2001)
17. J.R. Sambrano, L.A. Vasconcellos, J.B.L. Martins, M.R.C. Santso, E. Longo, A. Beltran, J. Mol. Struct., Theochem **629**, 307 (2003)
18. F.R. Sensato, R. Custodio, E. Longo, A. Beltrán, J. Andrés, Catal. Today **85**, 145 (2003)
19. J.R. Sambrano, G.F. No´brega, C.A. Taft, J. Andre´s, A. Beltra´n, Surf. Sci. **580**, 71 (2005)
20. F. Edelman, H. Hahn, S. Seifried, C. Alof, H. Hoche, A. Balogh, P. Werner, K. Zakrzewska, M. Radecka, P. Pasierb, A. Chack, V. Mikhelashvili, G. Eisenstein, Mater. Sci. Eng. B **69**, 386 (2000)
21. C. Wang, B.Q. Xu, J. Solid State Chem. **177**, 3448 (2004)
22. M. Radecka, P. Sobas, M. Rekas, Solid State Ion. **119**, 43 (1999)
23. J. Oviedo, M.J. Gillan, Surf. Sci. **490**, 221 (2001)
24. M. Radecka, K. Zakrzewska, M. Rekas, Sens. Actuators B **47**, 194 (1998)
25. M. Ferroni, M.C. Carotta, V. Guidi, G. Martinelli, F. Ronconi, M. Sacerdoti, E. Traversa, Sens. Actuators B **77**, 163 (2000)
26. K. Zakrzewska, M. Radecka, M. Rekas, Thin Solid Films **310**, 161 (1997)

27. J. Marien, T. Wagner, G. Duscher, A. Koch, M. Ruhle, Surf. Sci. **446**, 219 (2000)
28. K. Zakrzewska, Vacuum **74**, 335 (2004)
29. M.C. Carotta, M. Ferroni, V. Guidi, G. Martinelli, Adv. Mater. **11**, 943 (1999)
30. M.C. Carotta, M. Ferroni, D. Gnani, V. Guidi, M. Merli, G. Martinelli, M.C. Casale, M. Notaro, Sens. Actuators B **58**, 310 (1999)
31. M. Ferroni, M.C. Carotta, V. Guidi, G. Martinelli, F. Ronconi, O. Richard, D.V. Dyck, J. Van Landuyt, Sens. Actuators B **68**, 140 (2000)
32. N. Bonini, M.C. Carotta, A. Chiorino, V. Guidi, C. Mallagù, G. Martinelli, L. Paglialonga, M. Sacerdoti, Sens. Actuators B **68**, 274 (2000)
33. G. Martinelli, M.C. Carotta, E. Traversa, G. Ghiotti, Mater. Res. Bull. **24**(6), 30 (1999)
34. O.K. Tan, W. Cao, Y. Hu, W. Zhu, Ceram. Int. **30**, 1127 (2004)
35. Y. Shimizu, M. Egashira, Mater. Res. Bull. **24**(6), 18 (1999)
36. N. Barsan, U. Weimar, J. Electroceram. **7**, 143 (2001)
37. N. Kanai, T. Nuida, K. Ueta, K. Hashimoto, T. Watanabe, H. Ohsaki, Vacuum **74**, 723 (2004)
38. W.P. Tai, J.H. Oh, Sens. Actuators B **85**, 154 (2002)
39. O.K. Tan, W. Cao, Y. Hu, W. Zhu, Solid State Ion. **172**, 309 (2004)
40. L. Cao, H. Wan, L. Huo, S. Xi, J. Colloid Interface Sci. **244**, 97 (2001)
41. Q. Liu, X. Wu, B. Wang, Mater. Res. Bull. **37**, 2255 (2002)
42. M.A. López-Quintela, J. Quibén-Solla, J. Rivas, Surfactant Sci. Ser. **66**, 247 (2003)
43. T. Aukunprasert, C. Saiwan, E. Traversa, Sci. Technol. Adv. Mater. **6**, 359 (2005)
44. C. Saiwan, S. Krathong, T. Anukunprasert, E.A. O'Rear, J. Chem. Eng. Jpn. **37**, 279 (2004)
45. I. Capek, Adv. Colloid Interface Sci. **110**, 49 (2004)
46. R.K. Sharma, M.C. Bhatnagar, G.L. Sharma, Sens. Actuators B **46**, 194 (1998)
47. E. Traversa, M.L. Di Vona, S. Licocia, M. Sacerdoti, M.C. Carotta, L. Crema, G. Martinelli, J. Sol-Gel Sci. Technol. **22**, 167 (2001)
48. P. Knauth, H.L. Tuller, J. Appl. Phys. **85**, 897 (1999)
49. P. Knauth, H.L. Tuller, Solid State Ion. **136–137**, 1215 (2000)
50. A. Weibel, R. Bouchet, P. Knauth, Solid State Ion. **177**, 229 (2006)
51. Y.M. Chiang, E.B. Lavik, I. Kosacki, H.L. Tuller, J.Y. Ying, J. Electroceram. **1**, 7 (1997)
52. I. Kosacki, H.U. Anderson, Sens. Actuators B **48**, 263 (1998)
53. M. Koelsch, S. Cassaignon, C. Ta Thanh Minh, J.-F. Guillemoles, J.-P. Jolivet, Thin Solid Films **451**, 86 (2004)